Fusion of Structural and Functional Cardiac Magnetic Resonance Imaging Data for Studying Ventricular Fibrillation

K. Magtibay[1], M. Beheshti[1], F. H. Foomany[1], K. Balasundaram[1], S. Masse[2], P. Lai[2], J. Asta[2], N. Zamiri[2], D. A. Jaffray[3], K. Nanthakumar[2], S. Krishnan[1], and K. Umapathy[1]
[1]Ryerson University, [2]Toronto General Hospital, and [3]Princess Margaret Hospital
Toronto, Ontario, Canada

Abstract— **Magnetic Resonance Imaging (MRI) techniques such as Current Density Imaging (CDI) and Diffusion Tensor Imaging (DTI) provide a complementing set of imaging data that can describe both the functional and structural states of biological tissues. This paper presents a Joint Independent Component Analysis (jICA) based fusion approach which can be utilized to fuse CDI and DTI data to quantify the differences between two cardiac states: Ventricular Fibrillation (VF) and Asystolic/Normal (AS/NM). Such an approach could lead to a better insight on the mechanism of VF. Fusing CDI and DTI data from 8 data sets from 6 beating porcine hearts, in effect, detects the differences between two cardiac states, qualitatively and quantitatively. This initial study demonstrates the applicability of MRI-based imaging techniques and jICA-based fusion approach in studying cardiac arrhythmias.**

Index Terms **–Magnetic Resonance Imaging, Data Fusion, Ventricular Fibrillation, Joint Independent Component Analysis**

I. Introduction

Researchers have strived to understand the underlying mechanism of initiation, maintenance, and evolution of VF. In the past, they have undertaken a great deal of work in spatial and temporal characterization of VF - [1, 2, 3, & 4] to name a few - in order to track VF's organization and evolution. However, most studies on VF have been limited to the analysis of ventricular electrical activity on the surfaces of the epi- and endocardium. Although insightful, surface studies provide an incomplete depiction of VF's electrophysiology on a three-dimensional medium, that is, the mammalian heart. Therefore, the need to probe into the myocardium's internal bulk arises. Studies on VF using needle electrodes, such as [5], to study intramural activity of a heart during VF has been done however only specific regions on the myocardium were studied. In contrast, various medical imaging tools have been proven useful in providing greater depth of information from targeted anatomy and/or physiology in a non-invasive fashion.

In the case VF analysis, two known Magnetic resonance imaging (MRI) techniques could prove to be very useful: Current Density Imaging (CDI) and Diffusion Tensor Imaging (DTI). CDI, pioneered by [6], provides a spatial distribution of electrical currents passing through a medium. Images for CDI are obtained by computing the curl from the changes in magnetic flux caused by electrical currents [7]. On the other hand, DTI has been widely used to characterize the Brownian diffusion of water in tissues to provide exquisite details of tissue microstructure [8].

Both of these modalities can be used hand in hand in order to study the spatial distribution of electrical currents in the individual fibers of the myocardium during different modes of cardiac activation. In our previous work [9], we have established the existence of a greater correlation between the fibers of the myocardium along the superior-inferior (SI) axis and the curl of the magnetic flux along the same axis than the fibers along the anterior-posterior (AP) and medial-lateral (ML) axes.

Although complementary, these modalities are not readily fusible on a pixel level as they belong to different domains of measurement. Therefore, it is more reasonable to explore the information shared between these two modalities. A form of feature level fusion known as Joint Independent Component Analysis (jICA) has been developed by [10] to utilize the cross-information between two different but complementing modalities. In fact, jICA has been used for many different studies in the human brain to discover direct and remote associations on image and signal data while performing analyses on different human brain pathologies.

The objective of this paper is to discuss the utility of the jICA technique in fusing features of CDI and DTI, as used on porcine hearts, in order to gain better insight of the dynamics of VF by differentiating two cardiac states: VF and Asystolic/Normal (AS/NM) (AS and NM states are assumed to have similar electrical current pathways). Furthermore, the relationship between fibre orientation and electrical current distribution according to cardiac states shall be explored. On Section II, methodologies on data acquisition, CDI and DTI calculations, feature extraction, data pre-processing and fusion will be discussed. Subsequently, quantitative analyses and discussions on the results of fusion will be presented on Section III. Finally, Section IV outlines our conclusions from the study and list suggestions for further improvement.

II. Methods

A. Data Acquisition

Under an approved Animal Use Protocol drawn from Toronto General Hospital, 6 beating hearts were harvested from healthy porcine subjects while under deep anesthesia. From the Animal Resource Centre operating room, a heart was delivered to a nearby room where a mobile Lagendorff perfusion system (figure 1A) was set up.

This Research is supported by Ryerson University and Canadian Institute for Health Research (CIHR Grant Number: 111253) – Dr. K. Umapathy.

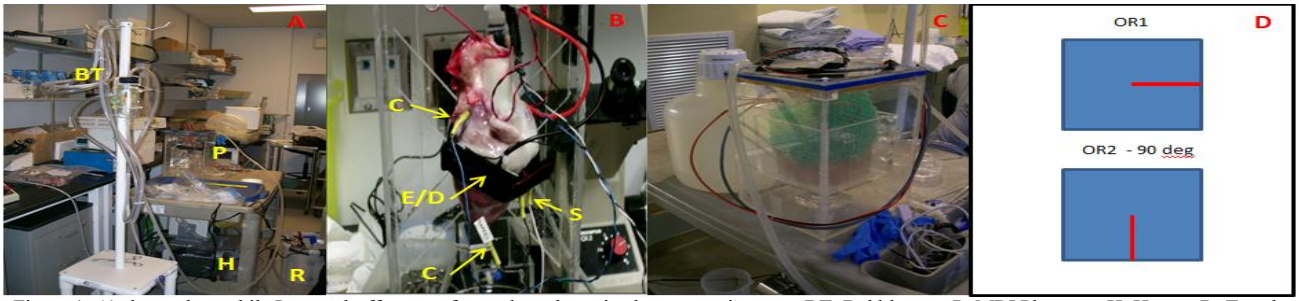

Figure 1: A) shows the mobile Langendorff system for explanted porcine heart experiments. : BT: Bubble trap; P: MRI Phantom; H: Heater; R: Tyrode reservoir. B) Depicts the electrode placements on a porcine pig before imaging. C: Current injection electrodes; S: Stimulation electrodes; E/D: ECG and Defibrillation copper pads. C) Shows the MRI phantom with the porcine heart inside which was fitted with bubble wrap to prevent sudden movements; A small, secondary bubble trap was set up inside the phantom D) Two orientations necessary for CDI collection as outlined in [11].

Using the equipment, a beating heart was perfused with carbogen-infused (95% O_2, 5% CO_2) Tyrode solution, maintained on an average temperature of 37°C. Non-magnetic electrodes were then attached to the myocardial sites as shown on figure 1B. The heart was placed inside a MRI phantom (figure 1C) to allow the Tyrode solution to circulate and protect the MRI machine. With the perfusion system, the beating heart was transported to the imaging wing of the hospital where our CDI protocols for two cardiac states were executed on a 1.5T GE Signa MRI System. Six (6) consecutive slices were collected from the ventricles of the heart with the following imaging parameters: NEX: 2-3; TR: 700 ms; TE: 40 ms; slice thickness: 7 mm; slice spacing: 0 mm; FOV: 15 cm; 2 Orientations (figure 1D); and current injection: 15 mA – 25 mA, depending on the heart's measured impedance. After the CDI protocols were completed, our DTI protocol was then executed on an asystolic heart with the same MRI system: Twenty-one (21) slices of diffusion-weighted images (DWIs) were collected from the entire heart with the following imaging parameters: NEX: 6; TR: 8300 ms; slice thickness: 7 mm; slice spacing: 0 mm; FOV: 15 cm; b value: 1000; and no. of directions: 30. Throughout the experiment, the heart's ECG was monitored. A batch of CDI images was eventually collected for each electrophysiological state of the heart (VF or AS/NM). DWIs were also collected after the CDI protocol has been executed and all electrodes have been removed. It is important to note that each cardiac state was treated as a separate "subject", even as the two states are from the same heart. In total, 8 datasets were collected from all 6 porcine hearts (4 subjects in a state of VF and 4 subjects in a state of AS/NM). Each experiment, lasting 3 to 5 hours in duration, required diligent and extensive preparation, coordination and collaboration with numerous departments.

B. CDI Calculation

The procedure in calculating CDI images are outlined in [11]. However, certain modifications were set in place to suit our application. With two orientations available, the curl of the magnetic flux (B) along the z-axis (J_z) can, thus, be calculated with the formula:

$$\mathbf{J_z} = \frac{1}{\mu_0}\left(\frac{\partial \mathbf{B_x}}{\partial \mathbf{y}} - \frac{\partial \mathbf{B_y}}{\partial \mathbf{x}}\right) \quad (1)$$

Where μ_0 is the permeability of free space and B_x and B_y are the magnetic flux components on the x and y axes respectively. Masks were created from the magnitude images by examining the histogram of each image and manually selecting the pixel value in which the histograms of the background and object intersect, serving as a threshold. A 5-by-5 median filter was applied after calculating the difference between the partial differentials in (1). J_z was then treated as a feature for CDI.

C. DTI Calculation

The DWI images collected were used as inputs to the 3D Slicer program in order to calculate the DTI images for each slice [12]. The components of the primary eigenvector of the diffusion tensor in each voxel were extracted. Since only the z-component of the overall curl of the magnetic flux in CDI was available, only the z-component of the primary eigenvector (D_z) was considered as a main feature for DTI.

D. CDI & DTI Slice Matching and Registration

A slice matching procedure was performed in the following way: the masks of six consecutive slices of CDI were matched to the Otsu masks [13] of the DTI images (obtained 3D Slicer) by taking the ratio each of the corresponding mask areas and calculating the variance among these ratios. The best matching set of Otsu masks should have the least variance compared to other sets. The matched slices were registered by cross correlating the masks of the matched images. With the coordinates of the maximum cross-correlation coefficient, the DTI images were shifted accordingly to match the spatial location of the CDI images. Manual inspection was carried out in order to ensure that a match was achieved between the two images.

E. Data Fusion – Joint Independent Component Analysis

jICA is a feature-based fusion technique, introduced by [10], that builds upon the idea that cross-information exists between different data sets. The goal is to estimate a joint de-mixing matrix, **W**, to estimate the components, **Y**, from the given mixture, **X**, that is

$$\mathbf{Y} = \mathbf{WX}. \quad (2)$$

W can be estimated such that the maximum likelihood of **W**, L(**W**), is maximized. If given data sets for CDI and DTI, X_C and X_D respectively, with dimensionalities N × P and N × Q respectively, then the likelihood function to be maximized can be written as follows [10]:

$$L(\boldsymbol{W}) = \prod_{n=1}^{N}\left(\prod_{p=1}^{P} p_{C,n}(u_{C,p}) \prod_{q=1}^{Q} p_{D,n}(u_{D,q})\right). \quad (3)$$

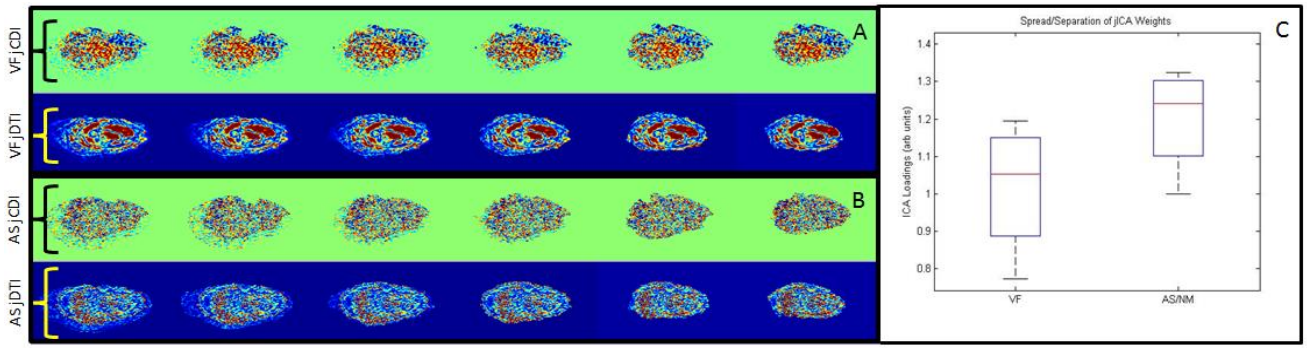

Figure 2: Results of jICA, fusing CDI and DTI image datasets. A) shows the reconstructed slices from a VF subject B) shows the reconstructed slices from an AS/NM subject. In both A & B, the top row represents the jCDI components and the bottom row represents the jDTI components. C) shows the jICA loadings obtained from the estimated demixing matrix, W; VF: $\mu = 1.02$, $\sigma = 0.18$, AS/NM: $\mu = 1.2$, $\sigma = 0.14$.

p_A and p_B are the probabilities of value $u_{C,p}$ and $u_{D,q}$, respectively. Each feature, J_z and D_z, were normalized to the maximum of the absolute value of the pixels within each slice so that the maximum value in a slice is 1. Following [14], as D_z carries only positive values, its pixel signs were adjusted in such a way that its mean was zero. This way, pixels with extremely small values were prevented from causing overwhelming contributions during fusion. For each subject, a slice of J_z and D_z images was concatenated side by side, with each slice stacked on top of each other, creating the matrix **P**. Principal Component Analysis (PCA) by Singular Value Decomposition (SVD), as explained on [15], was used to reduce the stack of images to one representative vector, $\mathbf{P}'$,

$$\mathbf{P}' = \mathbf{E}^{\boldsymbol{T}}\mathbf{P} \tag{4}$$

using the first right singular vector as the first principal component (**E**), conserving most of its variance. This was done for all 8 data sets. All representative vectors $\mathbf{P}'$were then stacked on top of each to form the feature matrix, **X**.

The Infomax Algorithm [16], was utilized to estimate a representative component for a subject (According to [17], Infomax was an equivalent of the maximum likelihood function used for data fusion in (3); hence, Infomax was used instead of a maximum likelihood algorithm). After estimating the component matrix (**Y**), each independent component ($\mathbf{Q}'$) for each subject were separated from the component matrix and the concatenated images (**Q**) were reconstructed using the same principal component used to reduce their dimension

$$\mathbf{Q} = \mathbf{E}\mathbf{Q}'. \tag{5}$$

The pixel signs on the reconstructed D_z were converted back to their original polarity. For each slice in both reconstructed J_z and D_z, corresponding masks were applied to eliminate pixel remnants from other subjects. Finally, for display, the means and standard deviations of each of reconstructed slices of J_z and D_z were calculated. The pixels were capped to a value equal to the mean, in addition to a multiple M (in this case, M = 3) of the standard deviation.

Following the convention established for jICA, the reconstructed J_z and D_z, will be labeled as jCDI and jDTI to denote joint CDI and joint DTI components.

In addition, from hereon in, the original CDI and DTI images will be labeled as oCDI and oDTI for ease of reference.

III. Results & Discussions

Figure 2 shows representative results of jICA for the VF group (2A), AS/NM group (2B), and the calculated jICA loadings (2C). From 2C, it could be observed that there is a qualitative difference between the two states highlighting the potential use of a jICA-based to fuse CDI and DTI data. For the quantitative comparison, a two sample t-test did not yield statistically significant results. However, this could be attributed to notably few samples.

In order to compare the advantages of fusing CDI and DTI using jICA and enhancing the difference between cardiac states, we also tested the differentiation of these two states using separate ICA loadings of CDI (Figure 3A) and DTI (Figure 3B). As seen in figures 3A and 3B, they did not yield observable difference between two cardiac states; this emphasizes the advantage of data fusion using the proposed

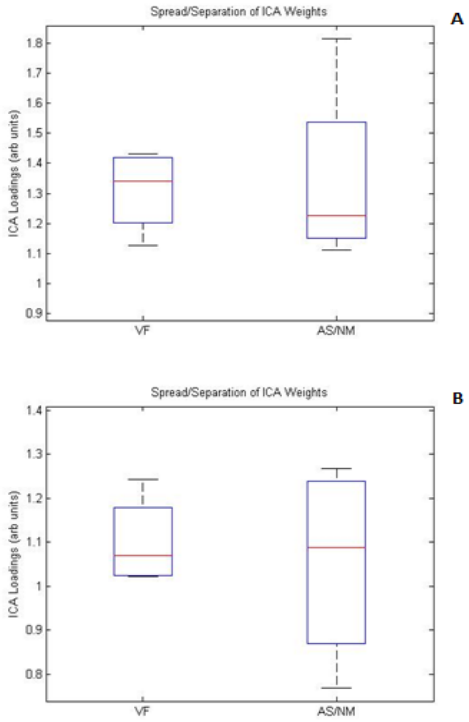

Figure 3: Separate ICA Loadings of CDI (A) and DTI (B) for two different cardiac states: VF and AS/NM. Instead of concatenating the two modalities, each had a feature matrix that was then demixed by infomax.

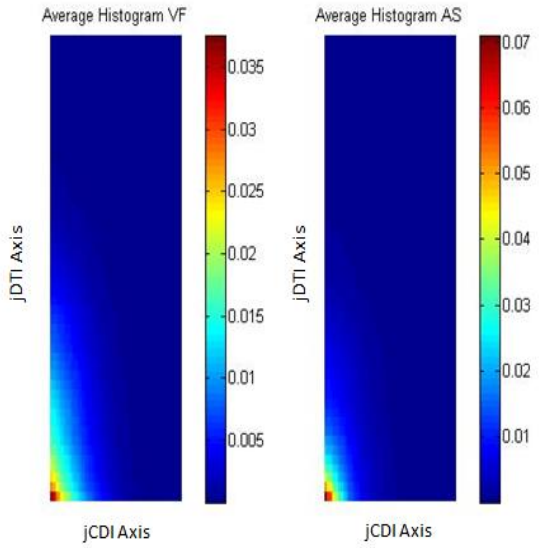

Figure 4: Joint Average Histograms of jCDI and jDTI computed across subjects for each cardiac state

approach. The relationship between jCDI and jDTI was also examined through the average joint histograms of the two cardiac states as shown on figure 4. It was found that for VF subjects there is a wider range of pixel values on both the jDTI and jCDI axes, as compared to concentrated pixel values for AS/NM subjects. In such a case, it is reasonable to suggest that, in the state of VF, more regions of the myocardium are active than in the state of AS/NM. Such areas can be located more easily on the jDTI images since these images project more distinct high intensity regions than the noisy jCDI images as shown on figure 2. Some of these regions can be seen on outer edges of the myocardium as well as in some places on the septum. In addition, these high intensity areas are also observed around where there is a build-up of Tyrode solution (usually in the ventricles).

It is important to note that we are assuming that DTI does not change with cardiac activity. Therefore, even though there is a considerable spread of pixel values on the jDTI axis for VF cases, the observed differences on the histograms are primarily influenced by the change in cardiac states captured by the original CDI images.

IV. Conclusions

This paper presented a jICA-based fusion for CDI and DTI data, combining the functional and structural characteristics of the cardiac tissue during VF and AS/NM. Using this approach we have demonstrated that fusion enhances the combined information from these two different imaging approaches which shows great potential in studying ventricular arrhythmias. Considering the complexity involved in the experimental procedures in obtaining data from an isolated heart set-up inside an MRI bore, the presented results prove to be encouraging. Future works involves increasing sample size, improving slice matching and image registration techniques, and testing the robustness of the jICA technique with additional cardiac data.

Acknowledgment

The authors would like to thank Mr. J. Koch for sharing his technical expertise during the development of our data acquisition tools. The authors would also like to thank Mr. N. Spiller for providing us time and assistance in our MRI experiments.

References

[1] J. Jalife, "Ventricular Fibrillation: Mechanisms of Initiation and Maintenance," *Annual Review of Physiology*, vol. 62, pp. 25-50, 2000

[2] J. Jalife, "Spatial and Temporal Organization in Ventricular Fibrillation," *Trends in Cardiovascular Medicince*, vol. 9, pp. 119 – 127, 1999.

[3] K. Umapathy, S. Masse, E. Sevaptisidis, J. Asta, H. Ross, N. Thavandiran, K. Nair, T. Farid, R. Cusimano, J. Rogers, S. Krishnan, and. K. Nanthakumar, "Regional Frequency Variation During Ventricular Fibrillation," *Medical Engineering & Physics*, vol. 31, pp. 964 – 970, 2009.

[4] K. Umapathy, S. Masse, E. Sevaptisidis, J. Asta, S. Krishnan, and K. Nanthakumar, "Spatiotemporal Frequency Analysis of Ventricular Fibrillation in Explanted Human Hearts," *IEEE Trans. Biomedical Engineering,* vol. 56, no. 2, pp. 328 – 335, 2009.

[5] K. Nair, K. Umapathy, T. Farid, S. Masse, E. Mueller, R.V. Sivanandan, K. Poku, V. Rao, V. Nair, J. Butany, R.E. Ideker, and K. Nanthakumar, "Intramural Activation During Early Human Ventricular Fibrillation," *Circulation: Arrhythmia and Electrophysiology*, vol. 4, no. 5, pp. 692 – 703, October 2011

[6] M. L. G. Joy, G. C. Scott, and R. M. Henkelman, "In-Vivo Detection of Applied Electric Currents by Magnetic Resonance Imaging," *Magnetic Resonance Imaging,* vol. 7, pp. 89 – 94, 1989.

[7] G. Scott, M. L. G. Joy, R. L. Armstrong, and R. M. Henkelman, "Measurement of Nonuniform Current Density by Magnetic Resonance," *IEEE Trans. on Medical Imaging*, vol. 10, no. 3, pp. 362 – 374, 1991.

[8] D. L. Bihan, J. F. Mangin, C. Poupon, C. A. Clark, S. Pappata, N. Molko, and H. Chabriat, "Diffusion Tensor Imaging: Concepts and Applications," *Journal of Magnetic Resonance Imaging,* vol. 13, pp. 534 – 546, 2001.

[9] F. H. Foomany, M. Beheshti, K. Magtibay, S. Masse, W. Foltz, E. Sevaptisidis, P. Lai, T. Farid, N. Krishnakumar, D. A. Jaffray, S. Krishnan, and K. Umapathy, "Correlating Current Pathways with Myocardial Fiber Orientation Through Fusion of Data from Current Density and Diffusion Tensor Imaging," *Canadian Journal of Cardiology*, vol. 28, no. 5, Supplement, pp. S372-S373, September 2012.

[10] V. D. Calhoun and T. Adali, "Feature-Based Fusion of Medical Imaging Data," *IEEE Trans. on Information Technology in Biomedicine*, vol. 13, no. 5, September 2009.

[11] T. DeMonte, "Low Frequency Current Density Imaging Cylindrical Phantom Experiment," University of Toronto, Toronto, ON, Tech. Rep. June 14, 2001.

[12] S. Pieper, M. Halle, and R. Kikinis, "3D Slicer," *Proceedings in IEEE International Symposium in Biomedical Imaging*, vol. 1, pp. 632 – 635, 2004.

[13] N. Otsu, "A Threshold Selection Method from Gray-Level Histograms," *IEEE Trans. on Systems, Man, and Cybernetics*, vol. 9, no. 1, pp. 62 – 66, Jan. 1979.

[14] V. D. Calhoun, T. Adali, N. R. Giuliani, J. J. Pekar, K. A. Kiehl, and G. D. Pearlson, "Method for Multimodal Analysis of Independent Source Differences in Schizophrenia: Combining Gray Matter Structural and Auditory Functional Data," *Human Brain Mapping*, vol 27, pp. 47-62, 2006.

[15] D. C. Lay, "Symmetric Matrices and Quadratic Forms," in *Linear Algebra and Its Applications*, 3rd ed. Maryland, USA: Pearson, 2006, ch. 7, sec.7.5. pp. 482 – 487.

[16] A. J. Bell and T. J. Sejnowski, "An Information-Maximisation Approach to Blind Separation and Blind Deconvolution," *Neural Computation*, vol. 7, no. 6, pp. 1004 – 1034, 1995.

[17] J. F. Cardoso, "Infomax and Maximum Likelihood for Blind Source Separation," *IEEE Signal Processing Letters*, vol. 4, no. 4, 1997.